Title page

Targeting endogenous K-RAS for degradation through the affinity-directed protein missile system

Sascha Röth[1], Thomas J. Macartney[1], Agnieszka Konopacka[2], Markus A. Queisser[2] and Gopal P. Sapkota*[1]

[1]Medical Research Council Protein Phosphorylation and Ubiquitylation Unit, University of Dundee, Dundee, United Kingdom. [2]GlaxoSmithKline, Protein Degradation Group, Medicines Research Centre, Gunnels Wood Road, Stevenage, UK.

*Correspondence and requests for materials should be addressed to: g.sapkota@dundee.ac.uk

Running Title: Targeted K-RAS proteolysis

ORCID IDs:

Sascha Röth: 0000-0001-7273-6701

Thomas J. Macartney: n.a.

Agnieszka Konopacka: 0000-0003-2192-1928

Markus A. Queisser: 0000-0002-3368-3827

Gopal P. Sapkota: 0000-0001-9931-3338

Abstract

For over three decades, *K-RAS* has been known as the holy grail of cancer targets, one of the most frequently mutated oncogenes in cancer. Because the development of conventional small molecule K-RAS inhibitors has been extremely challenging, K-RAS has been dubbed as an undruggable target, and only recently a mutation specific inhibitor has reached clinical trials. Targeted protein degradation has emerged as a new modality in drug discovery to tackle undruggable targets. However, no degrader for K-RAS has been described thus far. Our laboratory has developed an Affinity-directed PROtein Missile (AdPROM) system for targeted proteolysis of endogenous proteins through the ubiquitin proteasome system. Here, we show that we can achieve degradation of endogenous K-RAS and H-RAS in different cell lines in a targeted manner using our AdPROM system. Our findings imply that endogenous RAS proteins can be targeted for proteolysis, thereby offering tantalising possibilities for an alternative therapeutic approach to these so-called undruggable targets in cancer.

Keywords

High affinity binder, Ubiquitin proteasome system, UPS, Targeted proteolysis, PROTAC

Background

The three RAS oncogenes *H-RAS, K-RAS* and *N-RAS*, represent the most frequently mutated genes in cancer [1,2]. They encode four highly similar proteins, namely H-RAS, N-RAS, K-RAS4A and K-RAS4B, which undergo C-terminal farnesylation [3,4]. Farnesylation, in combination with palmitoylation in the hypervariable region (HVR) (N-RAS, H-RAS, K-RAS4A) or with a polybasic signal in the HVR (K-RAS4B), mediates the plasma membrane interaction [5]. RAS proteins are small GTPases, which cycle between the GTP-bound (active) and GDP-bound (inactive) states, controlled by guanosine nucleotide exchange factors (GEF) and GTPase activating proteins (GAPs) [6]. Activation of RAS proteins by various extracellular growth factors initiates activation of numerous downstream signalling networks, including BRAF/MAPK and PI3K pathways [7], that are critical for cell proliferation and viability. Many pathogenic mutations in *RAS* genes impair GAP mediated GTP hydrolysis, thereby favouring the persistence of the active RAS-GTP state, which triggers constitutive activation of downstream signalling resulting in unchecked proliferation of cancer cells [2,8].

As the oncogenicity of RAS mutations has been known for over three decades, intensive efforts have been made towards drugging them. These efforts are yet to result in effective RAS-inhibitor therapies [1,9]. This has promoted the perception that RAS proteins are undruggable. Several factors make RAS proteins difficult targets to engineer selective small molecule inhibitors. First, the relatively high concentrations of GTP and GDP in cells and picomolar affinity to binding RAS proteins makes it almost impossible to develop GTP/GDP analogues as inhibitors [1,10]. Second, structural analysis of RAS proteins revealed few sufficiently large and deep hydrophobic pockets on the surface for small molecule binding [11,12]. Recently, a covalent inhibitor

targeting a cysteine in K-RAS G12C was developed to target this specific mutation [13]. However, these barriers and failure to directly target RAS have prompted researchers to explore targeting upstream regulators, or downstream effectors of RAS proteins [1,9,14–16], as well as altering levels of RAS protein, for example by inducing targeted degradation of RAS [17].

Most targeted protein degradation approaches harness the cellular proteolytic pathways that naturally maintain proteostasis, with the ubiquitin-proteasome system (UPS) being frequently exploited [18]. Protein degradation by the UPS is triggered by conjugation of ubiquitin chains onto the target protein, which is achieved through a sequential action of three enzymes: the ubiquitin-activating enzyme (E1), which activates the carboxy-terminal glycine residue of ubiquitin in an ATP-dependent manner; a ubiquitin-conjugating enzyme (E2), which conjugates the activated ubiquitin to its active site cysteine; and a ubiquitin ligase (E3), which facilitates the transfer of ubiquitin from E2 to primarily lysine residues on substrate proteins [19,20]. Further ubiquitylation on one or more lysine residues within ubiquitin then triggers polyubiquitylation, followed by degradation by the proteasome [21–23]. Targeting RAS for proteolysis relies on the engagement of the cellular proteolytic systems for its ubiquitylation and degradation. In this context, it has been shown that the heterobifunctional molecule dTAG-13, which recruits FKBP12^{F36V}-tagged proteins of interest (POIs) to the CRBN/CUL4A E3 ubiquitin ligase for their degradation, can degrade FKBP12^{F36V}-KRAS^{G12V} overexpressed in cell lines [17]. However, FKBP12^{F36V} itself can be targeted for ubiquitylation when using heterobifunctional small molecule binders [24]. Therefore, it remains unclear, whether using dTAG13 on FKBP12^{F36V}-K-RAS results in the ubiquitination of K-RAS or FKBP12^{F36V}. Such information is not only key to evaluate proteolysis as a druggable approach for

targeting RAS proteins but also to inform on the development of effective heterobifunctional RAS degraders.

We have previously developed an effective proteolytic Affinity-directed PROtein Missile (AdPROM) system for UPS mediated POI degradation [25,26]. AdPROM consists of a fusion of von-Hippel-Lindau (VHL) protein, a substrate recruiter of the CUL2-RING E3 ligase complex, and high-affinity binders, such as nanobodies and monobodies, of POIs. Delivering AdPROM into multiple cell lines through retroviral transductions led to efficient degradation of endogenous target proteins, including SHP2 and ASC [26]. Furthermore, in order to target POIs for which no high-affinity polypeptide binders exist, we utilized CRISPR/Cas9 genome editing to rapidly introduce GFP tags on endogenous VPS34 and PAWS1 genes, and used the AdPROM system consisting of anti-GFP nanobody fused to VHL to achieve near-complete degradation of the endogenous GFP-VPS34 and PAWS1-GFP proteins [25]. In this study, we explore the use of the AdPROM system, and demonstrate its efficacy, for targeted degradation of endogenously GFP-tagged K-RAS and untagged, endogenous K-RAS from cells.

Methods

Sequence Alignment

Protein sequences of K-RAS4A/B, H-RAS and N-RAS were taken from Uniprot [27] and aligned in Clustal Omega [28]. The alignment was further processed in JalView [29] to highlight percent sequence identity.

RNA extraction, cDNA synthesis and qRT-PCR

For RNA extraction, $2x10_5$ cells were seeded in a 6-well dish and harvested the next day with the RNeasy Micro Kit (Qiagen, #74004) according to the manufacturer's protocol. 1 μg of RNA was reverse transcribed with the iScript cDNA synthesis Kit (BIORAD, #1708891) according to the manufacturer's protocol. For qRT-PCR 1 μl of diluted cDNA (1:20 or 1:80) was mixed with forward and reverse primers (Custom primers from Invitrogen, 300 nm final concentration each) and SsoFast EvaGreen Supermix (BIORAD, #1725204) in a 384-well plate (Axygen, #321-22-051) and run on a BIORAD CFX384.

Primer sequences:

K-RAS4A fw: GAGGGAGATCCGACAATACAG;

K-RAS4A rev: TCTCGAACTAATGTATAGAAGGCATC;

K-RAS4Bfw: TTGCCTTCTAGAACAGTAGACAC;

K-RAS4B rev: CATCGTCAACACCCTGTCTTG;

Total K-RAS fw: GGAGTACAGTGCAATGAGGG;

Total K-RAS rev: CCATAGGTACATCTTCAGAGTCC;

H-RAS fw: GAACAAGTGTGACCTGGCT;

H-RAS rev: ACCAACGTGTAGAAGGCATC;

N-RAS fw: AATACATGAGGACAGGCGAAG;

N-RAS rev: GTTTCCCACTAGCACCATAGG;

GAPDH fw: CTTTGTCAAGCTCATTTCCTGG;

GAPDH rev: TCTTCCTCTTGTGCTCTTGC.

Melting curves were analysed for purity of the PCR product and fold changes were calculated by the 2-ΔΔCt method [30].

Cell line maintenance and manipulation

All cells were cultured in humidified incubators at 37°C and 5% CO_2. A549, HEK293-FT, A375, A172 and SW620 cells were cultured in Dulbecco's modified Eagle's medium (DMEM; Gibco) with 10% FBS (Sigma), 1% penicillin/streptomycin (Lonza) and 2 mM L-glutamine (Lonza). HT-29, HPAFII and H460 cells were cultured in RPMI1640 medium (Gibco), with the same supplements as DMEM. For retrovirus production, 3.2 μg pCMV-gag-pol, 2.2 μg pCMV-VSV-G and 6 μg of respective pBabeD plasmids were co-transfected in roughly 70% confluent HEK293-FT cells cultured on a 10-cm dish. Plasmids were mixed with 600 μl Opti-MEM (Gibco) and 24 μl of 1 mg/ml polyethyleneimine (Polysciences) dissolved in 25 mM HEPES pH 7.5. The mixture was vigorously vortexed for 15 s and incubated for 20 min at room temperature. The volume was adjusted to 10 ml with DMEM and added to FT cells. After 24 h, medium was exchanged to DMEM or RPMI, depending on the target cell growth medium. After an additional 24 h, the medium was harvested and filtered through a 0.45 μm Minisart syringe filter (Sartorius). The supernatant was added to a plate of roughly 70% confluent target cells in a 1:10–1:4 dilution (in respective medium) in the presence of 8 μg/ml polybrene (Sigma). After 24 h, growth medium was exchanged with fresh medium containing 2 μg/ml puromycin, to select transduced cells. Puromycin was removed from the medium after 48 h.

Cells were lysed on ice, by washing once with PBS and scraping in lysis buffer (50 mM Tris–HCl pH 7.5, 0.27 M sucrose, 150 mM NaCl, 1 mM EGTA, 1 mM EDTA, 1 mM sodium orthovanadate, 1 mM sodium β-glycerophosphate, 50 mM sodium fluoride, 5 mM sodium pyrophosphate, 1% (v/v) Triton X-100 and 0.5% Nonidet P-40) supplemented with protease inhibitors (Roche; 1 tablet/25 ml of lysis buffer). Protein content from cleared cell lysates was determined with Pierce Detergent Compatible

Bradford Assay Kit (Thermo Fisher). Lysates were processed further or frozen and stored at -20°C.

CRISPR/Cas9

For generation of N-terminal GFP knock-in A549 cell lines the K-RAS locus was targeted with a dual guide approach [31] (using the sense guide (pBabeD vector, DU54976): GCGAATATGATCCAACAATAG; antisense guide (pX335 vector, DU54980): GCTGAATTAGCTGTATCGTCA; and the GFP-KRAS donor (pMK-RQ vector, DU57406). Briefly, 1 μg of each of the guideRNA plasmids and 3 μg of the donor plasmid were co-transfected into A549 cells. Plasmids were mixed with 1 ml of Opti-MEM (Gibco) and 20 μl of 1 mg/ml polyethyleneimine (Polysciences), vortexed vigorously for 15 s and added to 70% confluent cells in a 10-cm dish. The next day, cells were selected in puromycin (2.5 μg/ml) for 48 h and re-transfected with the same plasmids once they reached 70% confluence. Single GFP positive cells were obtained by FACS sorting and surviving single cell clones were screened by genomic DNA based PCR and western blot to validate homozygous knockin of the GFP-tag on the endogenous *KRAS* gene. For PCR based screening the following primers were used: Fw: ATCCAAGAGAACTACTGCCATGATGC;
Rv: CATGACCTTCAAGGTGTCTTACAGGTC. PCR products of positive clones were cloned with the StrataClone PCR Cloning Kit (Agilent) into the supplied vector system, according to the manufacturer's protocol. Sequencing of positive clones was carried out by the MRC-PPU DNA Sequencing and Services with a custom primer close to the RAS mutation site (Rv: CAAAGAATGGTCCTGCACCAG).

SDS PAGE and Western Blotting

Cell lysates were adjusted to uniform protein concentration and mixed with 6x reducing Laemmli SDS sample buffer (Fisher Scientific). 10-20 μg of total lysate protein, or immunoprecipitates were resolved by SDS polyacrylamide gel electrophoeresis (PAGE). After PAGE, proteins were transferred onto methanol activated PVDF membrane (Immobilon-P or Immobilon-FL, Merck) in Tris/glycine buffer containing 20% methanol in a tank blotting system for 85 min at a constant voltage of 85 V. The membranes were then re-incubated with methanol for 2 minutes and stained with Ponceau S solution to gauge uniform protein transfer (Sigma). After de-staining membranes in TBS-T (50 mM Tris–HCl pH 7.5, 150 mM NaCl, 0.1% Tween-20), they were blocked for 1 h in 5% non-fat milk (Marvel) in TBS-T. Primary antibody incubation was done overnight at 4°C in 5% milk/TBS-T. Following 3x10 min washes in TBS-T, membranes were incubated with respective HRP-conjugated (CST) or fluorescently labelled (Biorad) secondary antibodies for 1 h, washed again 3x10 min in TBS-T and developed on a ChemiDoc gel imaging system (Biorad) using the respective channels. HRP-conjugated blots were incubated with Immobilon Western Chemiluminescent HRP Substrate (Millipore).

Immunoprecipitation

Cell lysates were adjusted to 1 μg/μl in lysis buffer. Either GFP-trap beads (ChromoTek) or Anti-FLAG-M2-Affinity agarose resin (SigmaAldrich) was equilibrated with lysis buffer. 300-500 μg of total protein was added to 10-15 μl of beads (50% slurry) and incubated for an hour at 4°C under agitation. Centrifugation steps at 200xg were done at 4°C for 2 minutes. Supernatant (flowthrough) was separated from beads, and beads were washed 3-5 times in lysis buffer. Proteins were eluted in lysis buffer containing Laemmli SDS sample buffer by boiling at 95°C for 5 minutes.

225

226 **Antibodies**

227 Antibodies were purchased from Thermo Fisher (Alpha tubulin, MA1-80189; rat-HRP,
228 31470), Abcam (panRAS, ab206969; HIF1a, ab1), Sigma (K-RAS4B, WH0003845M1;
229 Flag-HRP, A8592-.2MG; GFP, 11814460001) CST (GAPDH, 2118S; rabbit-HRP,
230 7074S; mouse-HRP, 7076S) and Bio-Rad (rabbit starbright 700, 12004161). Primary
231 antibodies were generally used in 1:1,000 dilutions in 5% milk TBS-T, apart from RAS
232 (1:500), and GAPDH & alpha-tubulin (1:5,000). Secondary antibodies were used in a
233 1:5,000 dilution in 5% milk TBS-T. Other primary antibodies recognizing different RAS
234 species were obtained from Proteintech (N-RAS, 10724-1-AP; H-RAS, 18295-1-AP;
235 K-RAS2B, 16155-1-AP; K-RAS2A, 16156-1-AP) and Invitrogen (H-RAS, PA5-22392;
236 K-RAS, 415700).
237 Antibodies for immunofluorescence were purchased from MBL/Caltag Medsystems
238 (GFP, 598), Abcam (ATPB, ab14730), BD Biosciences (P120 Catenin, 610133),
239 Sigma (Flag-M2, F1804) and Thermo Fisher (AlexaFluor488 [donkey anti-rabbit],
240 A21206; AlexaFluor594 [goat anti-mouse], A11005).

241

242 **Immunofluorescence**

243 Cells were seeded in a 12-well dish onto cover slips and grown over night. The next
244 day, cells were washed twice in PBS and fixed for 10 minutes in 4%
245 formaldehyde/PBS (Sigma). Coverslips were washed in DMEM (Gibco) containing 10
246 mM HEPES followed by a 10 min incubation. Coverslips were washed in PBS and
247 permeabilised for 3 min in either 0.2% NP-40/PBS or 0.2% Triton X-100/PBS.
248 Coverslips were washed twice in PBS and blocked for 15 min in 3% BSA (Sigma) in
249 PBS. Primary antibody incubation was done for 1-2 h at room temperature at

appropriate antibody dilutions in blocking solution. Residual antibody was washed away in 0.2% Tween/PBS (3x10 min). Secondary antibody incubation was done for 30 min at 1:300 antibody dilution in the dark. The same wash steps were repeated, but the first wash contained DAPI (0.5–1 μg in 10 ml). Finally, coverslips were dipped in water, air dried and mounted on slides with Vectashield (Vector Laboratories). Fluorescence signals were analysed on a Deltavision Widefield microscope (GE). Images were deconvolved using the default settings of softWoRx Imaging software.

Cell Proliferation Assays

After trypsinization, live cell numbers were determined in a Neubauer haemocytometer in the presence of trypan blue. Cell numbers were adjusted to 5000 cells per ml in the respective growth medium. 5000 cells were added per well of a 12-well dish, and each line was grown in triplicates. After 7 days, relative cell numbers were determined by crystal violet staining. In short, cells were washed in PBS, fixed for 5 min in fixing buffer (10% methanol, 10% acetic acid), washed in PBS again and incubated for 30-60 min in crystal violet solution (0.5% crystal violet in 20% methanol). Plates were dipped in tap water to remove stain and air dried overnight. Plates were scanned on a Licor Odyssey using the 700 nm channel. Subsequently, 1 ml methanol was added to each well and plates were incubated shaking for 30 min. Depending on the colour of 1 set of cells, 100-200 μl of supernatant was loaded in triplicate on a 96-well plate and absorbance at 570 nm was measured in an Epoch microplate spectrophotometer (BioTek). Values were normalized to the untreated sample and a one-way ANOVA analysis with Dunnett's multiple comparisons test was done.

Flow Cytometric Analysis

Cells were trypsinized, washed and resuspended in PBS containing 1% FBS. Cells were then analysed on a FACS Canto II flow cytometer. Cells were analysed with the following gating strategy: (i) cells: in a plot of FSC-A vs. SSC-A, a gate was drawn surrounding the major population of cells, removing debris and dead cells. (ii) single cells: in a plot of FSC-A vs. FSC-W, a gate was drawn around an area corresponding to single cells. (iii) in the 'single cells' population on a GFP-A vs. PE-A plot a gate was drawn around GFP-positive cells in A549^{GFPKRAS} sample, using WT A549 cells as a negative control. Gates (i) and (ii) were adjusted to the individual cell lines. Gate (iii) was kept unchanged within an experiment.

Results

Generation of a GFP-KRAS knock-in non-small cell lung cancer A549 cell line

The high degree of amino acid sequence similarity between the four RAS proteins, i.e. K-RAS4A, K-RAS4B, H-RAS and N-RAS (Fig. 1A), and the subsequent difficulty in generating selective antibodies against individual isoforms pose substantial challenges in studying specific RAS proteins [32]. In order to explore targeted proteolysis of K-RAS using the AdPROM system, we employed CRISPR/Cas9 technology to generate an A549 non-small cell lung carcinoma (NSCLC) cell line harbouring a homozygous knock-in of green fluorescent protein (GFP) cDNA at the N-terminus of the native *K-RAS* gene (Fig. S1). As K-RAS4A and K-RAS4B are splice variants differing only in their extreme C-terminus (Fig. 1A), this approach allowed us to simultaneously tag both isoforms with GFP. The homozygous GFP knock-ins on the native K-RAS locus (A549^{GFPKRAS}) were verified by genomic sequencing (Fig. S1). Moreover, by western blot analysis using both pan-RAS and K-RAS4B antibodies, the appearance of higher molecular weight GFP-K-RAS species with a concurrent

disappearance of the native molecular weight K-RAS species was evident in the A549^{GFPKRAS} cell line compared to wild type (WT) A549 control cells (Fig. 1B). The use of a panRAS antibody resulted in the detection of two distinct bands in A549 WT cells (Fig.1B). As the lower band remained intact in A549^{GFPKRAS} cells, it most likely corresponds to H- and/or N-RAS (Fig. 1B). However, in A549 cells we were unable to detect any endogenous signals with commercially available H-RAS, N-RAS or K-RAS4A specific antibodies (listed in Methods section). By qRT-PCR, we showed that levels of H- and N-RAS transcripts were slightly reduced in A549^{GFPKRAS} cells compared to WT A549 cells, while transcript levels of K-RAS were reduced by roughly 50% (Fig. S2). We were able to efficiently immunoprecipitate GFP-K-RAS from A549^{GFPKRAS} but not WT A549 cell extracts (Fig. 1C).

Recently, a number of RAS antibodies have been evaluated for selective recognition of the different RAS proteins by Western blotting [32], but none of these have been selective for use in immunofluorescence studies. Consequently, studies evaluating subcellular distribution of RAS proteins have been restricted to overexpression systems. Validation of A549^{GFPKRAS} cells allowed us to investigate the sub-cellular distribution of endogenous GFP-K-RAS driven by the native promoter. Endogenous GFP-K-RAS displayed predominantly plasma membrane distribution, which was confirmed by co-staining with P120 catenin, which is known to localise to the plasma membrane [33] (Fig. 1D, Fig. S3). Additionally, we also observed some weak cytoplasmic localisation of GFP-K-RAS. However, no co-localisation of GFP-K-RAS was observed with mitochondrial marker ATPB [34] (Fig. 1D, Fig. S3).

Targeted degradation of GFP-K-RAS by the proteolytic AdPROM system

We sought to test whether endogenously expressed GFP-K-RAS protein in A549^{GFPKRAS} cells could be targeted for degradation by AdPROM [25,26]. We have previously shown that fusion of VHL to an aGFP16 nanobody recruits GFP-tagged proteins, such as VPS34 and PAWS1, to the CUL2-RBX1 E3 ligase machinery for target ubiquitination and subsequent proteasomal degradation [25]. Therefore, we postulated that GFP-K-RAS could be recruited in a similar manner to the CUL2-RBX complex for ubiquitination and degradation (Fig. 2A). Indeed, expression of VHL-aGFP16 AdPROM resulted in near complete clearance of GFP-K-RAS from A549^{GFPKRAS} cells compared to the untransduced controls, while the low molecular weight band corresponding to H- and/or N-RAS was unaffected (Fig. 2B). In contrast, neither VHL nor the aGFP16 nanobody alone, serving as controls, caused any apparent changes in the steady state levels of GFP-K-RAS or other RAS proteins (Fig. 2B). Treatment of VHL-aGFP16 AdPROM expressing A549^{GFPKRAS} cells with the Cullin neddylation inhibitor MLN4924 partially rescued the degradation of GFP-K-RAS compared to DMSO-treated controls (Fig. 2C). The neddylation of CUL2 allows a conformational change of the CUL2-RBX E3 ligase machinery so that the RBX E3 ligase is able to ubiquitinate substrates recruited by VHL. In line with this notion, the levels of HIF1α protein, a *bona fide* substrate of VHL [35], were stabilized upon MLN4924 treatment compared to DMSO control (Fig. 2C). Despite the high apparent efficiency of GFP-KRAS degradation by VHL-aGFP16 AdPROM, the retroviral transduction of A549^{GFPKRAS} cells often generates uneven levels of AdPROM expression in a mixed population of cells. Therefore, in order to get a better understanding of the distribution of the cells within this population, we employed a flow cytometric analysis based on GFP fluorescence. We employed gates to define a GFP-positive population based on the GFP-signal from untransduced A549^{GFPKRAS} cells and

using WT A549 cells as a GFP-negative control (Fig. 2D). In accordance with the Western blot results (Fig. 2B), 97% of cells expressing VHL-aGFP16 AdPROM showed GFP-KRAS degradation compared to untransduced A549^{GFPKRAS} cells (Fig. 2D), which manifested in an overall reduction of GFP fluorescence of the single cell population (Fig. 2E). The remaining 3% of A549^{GFPKRAS} cells produced GFP signal comparable to untransduced GFP-positive-population, which could be due to low level AdPROM expression within these cells (Fig. 2D). In contrast, A549^{GFPKRAS} cells expressing VHL or aGFP16 alone were defined as GFP-positive at 99.3% or 99.8%, respectively (Fig. 2D, E).

AdPROM mediated degradation of endogenous RAS proteins

The AdPROM-mediated degradation of GFP-K-RAS in A549^{GFPKRAS} cells demonstrated the prospect of targeted degradation of endogenous K-RAS. However, the presence of the GFP-tag raised the possibility of ubiquitination occurring on the GFP moiety, instead of on K-RAS. Therefore, we sought to explore whether we could exploit the AdPROM system to degrade endogenous, unmodified K-RAS from A549 cells. At present, there are no reported high affinity, selective polypeptide binders of K-RAS. However, we utilized an anti-H-RAS (aHRAS) monobody that was reported to bind and immunoprecipitate both H-RAS and K-RAS, but not N-RAS [36]. Using this monobody with a FLAG-tag, we showed that anti-FLAG immunoprecipitates (IPs) could robustly coprecipitate both GFP-tagged and untagged K-RAS, as well as the lower molecular weight protein representing the H- and/or N-RAS band but most likely to be H-RAS [36] (Fig. 3A). However, neither RAS protein was completely depleted from flow-through extracts, suggesting incomplete immunoprecipitation (Fig. 3A). In

374 contrast, anti-FLAG IPs from extracts expressing Flag-VHL control did not co-
375 precipitate either protein (Fig. 3A).
376
377 Next, we sought to investigate whether AdPROM consisting of VHL fused to aHRAS
378 monobody could target K- and H-RAS proteins for degradation. In A549^{GFPKRAS} cells,
379 the expression of VHL-aHRAS resulted in a strong reduction of the GFP-K-RAS
380 protein levels when compared to untransduced, VHL or monobody alone controls (Fig.
381 3B). However, the degradation induced by VHL-aHRAS AdPROM was slightly less
382 efficient than that achieved with the VHL-aGFP16 AdPROM (Fig. 3B). Unlike VHL-
383 aGFP16, VHL-aHRAS also reduced the protein levels corresponding to the H-RAS
384 and/or N-RAS band (Fig. 3B). The loss in protein levels of endogenous H-RAS protein
385 caused by VHL-aHRAS AdPROM could be rescued by the Cullin neddylation inhibitor
386 MLN4924, suggesting that the degradation was mediated through CUL2-RBX E3
387 ligase machinery (Fig. 3C). As expected, MLN4924 also stabilised endogenous HIF1α
388 (Fig. 3C). We also assessed the relative abundance of GFP-K-RAS in mixed
389 populations of A549^{GFPKRAS} cells transduced with VHL-aHRAS AdPROM in
390 comparison to controls by flow cytometry. We found that 77% of cells showed
391 degradation of GFP-K-RAS, as assessed by the shift of the GFP-positive gated
392 population towards the GFP-negative population (Fig. 3D) and the overall reduction of
393 GFP-signal (Fig. 3E). The remaining 23% of cells transduced with VHL-aHRAS were
394 seemingly unaffected in both positioning in the GFP-positive gate (Fig. 3D), as well as
395 GFP intensity (Fig. 3E). Transductions with VHL or aHRAS alone did not induce a
396 noticeable shift of the GFP population or GFP signal intensity (Fig. 3D & E).
397

Uneven retroviral transduction of cells could result in unequal expression of the AdPROM constructs in different cells resulting in a mixed, divergent cell population, which may account for the apparent uneven degradation of GFP-K-RAS through VHL-aHRAS. When we analysed these A549^{GFPKRAS} mixed cell populations by immunofluorescence for GFP signal, in untransduced and aHRAS-transduced control cells, a predominant plasma membrane GFP-K-RAS signal was evident (Fig. 3F). Transduction of A549^{GFPKRAS} cells with either VHL-aHRAS or VHL-aGFP16 AdPROM produced a heterogenous population comprising cells with missing or severely attenuated GFP signal, and cells with intact GFP-K-RAS staining pattern, localizing mainly to the plasma membrane (Fig. 3F). In contrast, we noticed a slight increase in perinuclear GFP-K-RAS signal in cells transduced with the aHRAS monobody alone (Fig. 3F). Interestingly, we detected that the majority of the monobody itself was in the nucleus (Fig. S4), while we were unable to consistently detect signals for the AdPROM fusion proteins by anti-FLAG immunofluorescence (Fig. S4).

We also tested the degradation of endogenous K- and H-RAS in WT A549 cells with VHL-aHRAS AdPROM. The transduction of cells with VHL-aHRAS resulted in a substantial reduction in apparent levels of both K-RAS (upper band) and H-RAS (lower band) proteins as detected by the pan-RAS antibody compared to untransduced controls (Fig. 3G). Unlike in A549^{GFPKRAS} cells (Fig. 3B), WT cells transduced with VHL-aGFP16 AdPROM did not have any noticeable effect on K-RAS and H-RAS protein levels relative to untransduced cells (Fig. 3G), further validating the targeted nature of RAS degradation by AdPROM. Cells transduced with the aHRAS monobody alone led to a slight increase in abundance of both K-RAS and H-RAS proteins compared to untransduced controls (Fig. 3G). We sought to explore whether targeted

degradation of K- and H-RAS proteins from WT A549 cells using the VHL-aHRAS AdPROM, and GFP-K-RAS from A549^{GFPKRAS} cells using the VHL-aGFP16 AdPROM would impact cell proliferation. No significant differences in proliferation could be observed for either WT A549 or A549^{GFPKRAS} cells following AdPROM-mediated degradation of the respective RAS proteins compared to controls after 7 days, as measured by crystal violet staining (Figs. 3H & I). Although A549 cells harbour the oncogenic K-RAS^{G12S} mutation, they also harbour over 250 genetic mutations (COSMIC cell lines project), including some known oncogenes and tumour suppressors reducing the likelihood that these cells are solely dependent on the K-RAS^{G12S} oncogene for their proliferation.

Expansion of the RAS-targeting AdPROM system in different cell lines

Having demonstrated for the first time that the VHL-aHRAS AdPROM system could target endogenous H- and K-RAS for degradation in A549 cells, we sought to explore whether the system would work in other cell lines. First, we compared different cell lines for their endogenous RAS protein expression (Fig. 4A) relative to A549 cells. All cells tested displayed K-RAS protein expression similar to or slightly lower than A549 cells. SW620 cells, which harbour the G12V mutation on K-RAS [37], displayed similar levels of expression to A549 cells, however, we noticed that K-RAS in this cell line produced a slight but noticeable molecular weight shift, when probed with panRAS and K-RAS4B antibodies (Fig. 4A). Protein levels corresponding to the lower H- and/or N-RAS band were similar in all lines tested but overall much lower in intensity than that seen for K-RAS. We tested the ability of VHL-aHRAS AdPROM to degrade RAS proteins from HT-29 and SW620 cells. In HT-29 cells, which express WT RAS proteins but harbour the activating BRAF V600E mutation [38], only the levels of H-RAS but

not K-RAS proteins were reduced by VHL-aHRAS AdPROM compared to controls (Fig. 4B, left panel). The proliferation of HT-29 cells was only reduced by about 50% by the aHRAS monobody alone (Fig. 4C and D), while the VHL-aHRAS and VHL-aGFP16 constructs reduced growth to a lesser extent (Fig. 4D, left panel). For SW620 cells, which harbour the G12V mutation of K-RAS, we noticed a high K-RAS signal to H-/N-RAS signal ratio, as the latter was barely detectable (Fig. 4B, right panel). We observed stabilization of K-RAS with the aHRAS monobody alone, while VHL-aHRAS failed to degrade K-RAS compared to controls. Interestingly, both the aHRAS monobody alone and the VHL-aHRAS AdPROM but not VHL-aGFP16 AdPROM were able to reduce the proliferation of SW620 cells significantly by about 50% (Fig. 4C & D).

Discussion

In this report, we demonstrate that endogenous K-RAS and H-RAS proteins can be targeted for degradation using the proteolytic AdPROM system. RAS proteins have remained elusive targets for anti-cancer therapies, primarily due to their undruggability [1]. Research into obtaining small molecule inhibitors of K-RAS has been carried out for over 30 years without much success [39]. Recently, RAS targeting small molecules have emerged, with specificities to (i) a specific mutation status of K-RAS (G12C), i.e. ARS-1620 [40], and ARS-853 [41]; (ii) K-RAS, independent of the mutation status [42]; or (iii) RAS proteins in either nucleotide binding state [43]. Two compounds targeting K-RAS$_{G12C}$ mutation, AMG510 and MRTX849, are currently undergoing clinical trials [44]. An alternative approach has been the development of high affinity polypeptide binders of RAS that neutralise the RAS function. A class of binders based on ankyrin repeat proteins (DARPINs) [45] can bind and neutralise specific nucleotide loading

states of RAS proteins [45]. Similarly, a fibronectin type III domain-based RAS-binding monobody [36,46–48] was shown to bind and inhibit the dimerization of both K- and H-RAS, and the overexpression of this monobody was shown to suppress tumour growth in mice [48]. Besides inhibition, RAS degradation offers another alternative approach at inhibiting RAS function to target RAS-dependent cancer cells. In this context, the dTAG-13 PROTAC was used to degrade $FKBP12^{F36V}$-tagged K-RAS [17] through the UPS, albeit when overexpressed in cells. Our AdPROM system, demonstrating here that endogenous RAS proteins can be targeted for proteolysis through the UPS, informs that small molecules targeting RAS proteins for degradation is a viable option for intervention. Furthermore, our $A549^{GFPKRAS}$ cells provide an excellent high throughput screening platform to test the efficacy of such molecules. However, targeted delivery of polypeptide binders of RAS proteins or the proteolytic AdPROM system into RAS-dependent cancer cells remains challenging and therefore currently offers limited therapeutic potential.

One difficulty in the study of RAS proteins is the absence of robust reagents to reliably detect specific RAS proteins at the endogenous levels, especially by immunofluorescence [32]. Often, overexpression of GFP-tagged or other epitope-tagged K-RAS has been employed to investigate RAS localization [36,49,50]. Therefore, our homozygous $A549^{GFPKRAS}$ NSCLC cell line generated using CRISPR/Cas9, notwithstanding the potential caveats of GFP-tagging, has allowed us to not only assess localization of endogenously driven GFP-K-RAS protein but its mobility shift has allowed us to test the utility of panRAS and K-RAS antibodies in detecting K-RAS by Western blotting. Beyond the plasma membrane localisation, we observed additional disperse cytoplasmic signals of endogenous GFP-K-RAS, but no

mitochondrial localisation. When overexpressed, K-RAS$_{G12V}$ has been implied to be transported into mitochondria, leading to alterations of membrane potential, a decrease in respiration and an increase in glycolysis [51]. Potential compartments for the observed cytosolic signal for K-RAS could be Golgi, as seen for H- and N-RAS [52], which could correspond to K-RAS4A signal, or Endoplasmic Reticulum. However, this remains to be verified.

While the VHL-aGFP AdPROM was very effective at selectively degrading GFP-K-RAS from A549^{GFPKRAS} cells, the VHL-aHRAS AdPROM degraded endogenous H- and K-RAS with mixed efficacy in different cell lines. In developing the aHRAS monobody, the authors noted a difference in downstream behaviours of H- and K-RAS upon monobody binding, such as K-RAS, but not H-RAS being displaced from the membrane, or the mutant K-RAS, but not mutant H-RAS interaction with RAF being disturbed by monobody binding [46]. The full determinants of interaction between the aHRAS monobody and different H- and K-RAS mutants or any post-translationally modified forms remain poorly defined. It is perhaps the differences in affinity between the RAS proteins and the aHRAS monobody that define how robustly or poorly VHL-aHRAS can degrade different RAS proteins. Nonetheless, our study proves that any high-affinity polypeptide binders that can selectively bind specific RAS proteins or mutants can be packaged with VHL-AdPROM in order to target specific RAS proteins for proteasomal degradation. We also noted that aHRAS monobody alone resulted in a marked stabilization of both H-RAS and K-RAS in multiple cells (Fig. 3G & F and Fig. 4B), which could be caused either by a feedback loop induced by the inhibition of both RAS species imparted by aHRAS binding, or by blocking the natural turnover

pathway through binding the RAS dimerization interface at helical structures α4-α5 [36].

For the cell lines that we used, AdPROM-mediated degradation of H-/K-RAS was not sufficient to induce inhibition of anchorage-dependent cell proliferation. For A549 cells that are considered not to be K-RAS-dependent for proliferation, this is perhaps not surprising [53,54]. Meanwhile, SW620 cells have been reported to be K-RAS dependent for proliferation [55], however, their proliferation was inhibited by aHRAS monobody alone and the VHL-aHRAS AdPROM, which caused no detectable degradation of K-RAS, did not inhibit their proliferation any further. The inhibition of cell proliferation of RAS-dependent cells by aHRAS monobody is consistent with previous reports [36,48]. The lack of degradation of K-RAS by VHL-aHRAS AdPROM could be due to the unusual size shift of K-RAS in these cells, possibly caused by a post-translational modification or a mutation that might allow binding to aHRAS monobody but prevent ubiquitylation by the VHL-AdPROM, although this needs to be defined further. Many RAS-dependent cell proliferation assays employ anchorage-independent 3D cultures. For example, the K-RAS$_{G12C}$ drug ARS-1620 was shown to be effective at inhibiting RAS-dependent cell proliferation in 3D cultures but not in 2D cultures [40]. In order to assess the effects of AdPROM-mediated degradation of H-/K-RAS on proliferation robustly, it will be essential to first obtain polypeptide RAS binders that bind to specific RAS proteins with high affinity and then use them in RAS-dependent cell lines using 3D proliferation assays.

Recently two allosteric small molecule binders were described for K-RAS with low micromolar and nanomolar binding affinities [42,43]. It would be important to test these

binders' capabilities as K-RAS targeting warheads in a PROTAC approach. In this line, a re-evaluation of RAS binding molecules, with or without inhibitory function, might prove successful for PROTAC designs.

Conclusion

Our findings demonstrate clearly that endogenous RAS proteins can be targeted for proteasomal degradation by employing the AdPROM system. The system is not only suitable for studying the functions of these RAS proteins but also unequivocally informs that targeted proteolysis of endogenous K-RAS is a viable strategy to target K-RAS-dependent pathologies. The findings open up exciting opportunities to develop VHL-recruiting K-RAS-specific cell-permeable PROTACs as potential therapeutic agents. Our findings also highlight the need for developing better and more selective RAS binding polypeptides, such as nanobodies or monobodies, to achieve more selective degradation with the AdPROM system.

List of abbreviations

AdPROM – Affinity directed PROtein Missile

ASC – Apoptosis-associated speck-like protein containing a CARD

ATPB – ATP synthase subunit β

BRAF – B – Rapidly Accelerated Fibrosarcoma

Cas9 – CRISPR associated protein 9

CRBN – Cereblon

CRISPR – Clustered Regularly Interspaced short palindromic repeats

CUL – Cullin

DAPI – 4,6-diamidino-2-phenylindole

572 DARPIN – Designed Ankyrin Repeat Protein

573 FACS – Fluorescence Activated Cell Sorting

574 FKBP – FK506 Binding Protein

575 GAP – GTPase Activating Protein

576 GAPDH – Glyceraldehyde 3-phosphate dehydrogenase

577 GDP – Guanosine diphosphate

578 GEF – Guanosine Nucleotide Exchange Factor

579 GFP – Green Fluorescent Protein

580 GTP – Guanosine triphosphate

581 HIF1α - Hypoxia Inducible Factor 1α

582 HVR – Hypervariable region

583 MAPK – Mitogen Activated Protein Kinase

584 NSCLC – Non-small cell lung carcinoma

585 PAWS1 – Protein associated with Smad1

586 PI3K – Phosphoinositide 3-kinase

587 qRT-PCR – Real-time quantitative RT-PCR

588 RAS – Rat Sarcoma

589 RBX1 – RING box protein 1

590 SDS-PAGE – SDS Polyacrylamide Gel Electrophoresis

591 SHP2 – Src homology region 2 (SH2)-containing protein tyrosine phosphatase 2

592 UPS – Ubiquitin Proteasome System

593 VHL – Von-Hippel-Lindau

594 VPS34 – Vacuolar protein sorting 34

595

596 **Declarations**

Ethics approval and consent to participate

Not applicable

Consent for publication

Not applicable

Availability of data and materials

All data generated and analysed during this study is currently available in the Center for Open Science repository under the following link, https://osf.io/g5qn9/?view_only=4ef0cf7df11f4174b5f6760fa10042fe

Data will be stored as permanent registry and publicly available upon acceptance of the manuscript.

Competing interests

The authors declare that they have no competing interests

Funding

SR is supported by GlaxoSmithKline through the Division of Signal Transduction Therapy collaboration. AK and MQ are employees of GlaxoSmithKline. GPS is supported by the UK MRC (Grant MC_UU_12016/3) and the pharmaceutical companies supporting the Division of Signal Transduction Therapy (Boehringer-Ingelheim, GlaxoSmithKline, Merck-Serono).

Authors' contributions

TJM generated all used plasmids. SR, AK, MAQ and GPS designed the project. SR and GPS drafted the manuscript. SR acquired and analysed the data. SR and GPS interpreted the data.

Acknowledgements

We thank GS laboratory members for their highly appreciated experimental advice and/or discussions during the course of these experiments. We thank L. Fin, E. Allen,

J. Stark and A. Muir for help and assistance with tissue culture, the staff at the DNA Sequencing services (School of Life Sciences, University of Dundee), and the cloning teams within the MRC-PPU reagents and services (University of Dundee), coordinated by J. Hastie and H. McLauchlan. We thank the staff at the Dundee Imaging Facility (School of Life Sciences, University of Dundee), and the staff at the flow cytometry facility (School of Life Sciences, University of Dundee) for their invaluable help and advice throughout this project.

References

[1] Cox AD, Fesik SW, Kimmelman AC, Luo J, Der CJ. Drugging the undruggable RAS: Mission Possible? Nat Rev Drug Discov 2014;13:828–51. doi:10.1038/nrd4389.

[2] Hobbs GA, Der CJ, Rossman KL. RAS isoforms and mutations in cancer at a glance. J Cell Sci 2016;129:1287–92. doi:10.1242/jcs.182873.

[3] Schaber MD, O'Hara MB, Garsky VM, Mosser SD, Bergstrom JD, Moores SL, et al. Polyisoprenylation of Ras in Vitro by a Farnesyl-Protein Transferase. J Biol Chem 1990;265:14701–4.

[4] Reiss Y, Goldstein JL, Seabra MC, Casey PJ, Brown MS. Inhibition of purified p21ras farnesyl:protein transferase by Cys-AAX tetrapeptides. Cell 1990;62:81–8. doi:10.1016/0092-8674(90)90242-7.

[5] Ahearn IM, Haigis K, Bar-Sagi D, Philips MR. Regulating the regulator: post-translational modification of RAS. Nat Rev Mol Cell Biol 2012;13:39–51. doi:10.1038/nrm3255.

[6] Vigil D, Cherfils J, Rossman KL, Der CJ. Ras superfamily GEFs and GAPs: validated and tractable targets for cancer therapy? Nat Rev Cancer

2010;10:842–57. doi:10.1038/nrc2960.

[7] Khan AQ, Kuttikrishnan S, Siveen KS, Prabhu KS, Shanmugakonar M, Al-Naemi HA, et al. RAS-mediated oncogenic signaling pathways in human malignancies. Semin Cancer Biol 2019;54:1–13. doi:10.1016/j.semcancer.2018.03.001.

[8] Marcus K, Mattos C. Direct Attack on RAS: Intramolecular Communication and Mutation-Specific Effects. Clin Cancer Res 2015;21. doi:10.1158/1078-0432.CCR-14-2148.

[9] Papke B, Der CJ. Drugging RAS: Know the enemy. Science 2017;355:1158–63. doi:10.1126/science.aam7622.

[10] John J, Sohmen R, Feuerstein J, Linke R, Wittinghofer A, Goody RS. Kinetics of interaction of nucleotides with nucleotide-free H-ras p21. Biochemistry 1990;29:6058–65. doi:10.1021/bi00477a025.

[11] O'Bryan JP. Pharmacological targeting of RAS: Recent success with direct inhibitors. Pharmacol Res 2019;139:503–11. doi:10.1016/j.phrs.2018.10.021.

[12] Pai EF, Kabsch W, Krengel U, Holmes KC, John J, Wittinghofer A. Structure of the guanine-nucleotide-binding domain of the Ha-ras oncogene product p21 in the triphosphate conformation. Nature 1989;341:209–14. doi:10.1038/341209a0.

[13] Ostrem JM, Peters U, Sos ML, Wells JA, Shokat KM. K-Ras(G12C) inhibitors allosterically control GTP affinity and effector interactions. Nature 2013;503:548–51. doi:10.1038/nature12796.

[14] Leung ELH, Luo LX, Liu ZQ, Wong VKW, Lu LL, Xie Y, et al. Inhibition of KRAS-dependent lung cancer cell growth by deltarasin: blockage of autophagy increases its cytotoxicity. Cell Death Dis 2018;9:216. doi:10.1038/s41419-017-

0065-9.

[15] Waldmann H, Karaguni I-M, Carpintero M, Gourzoulidou E, Herrmann C, Brockmann C, et al. Sulindac-Derived Ras Pathway Inhibitors Target the Ras–Raf Interaction and Downstream Effectors in the Ras Pathway. Angew Chemie Int Ed 2004;43:454–8. doi:10.1002/anie.200353089.

[16] Kang S, Kim E-S, Moon A. Simvastatin and lovastatin inhibit breast cell invasion induced by H-Ras. Oncol Rep 2009;21:1317–22. doi:10.3892/or_00000357.

[17] Nabet B, Roberts JM, Buckley DL, Paulk J, Dastjerdi S, Yang A, et al. The dTAG system for immediate and target-specific protein degradation. Nat Chem Biol 2018;14:431–41. doi:10.1038/s41589-018-0021-8.

[18] Röth S, Fulcher LJ, Sapkota GP. Advances in targeted degradation of endogenous proteins. Cell Mol Life Sci 2019;76:2761–77. doi:10.1007/s00018-019-03112-6.

[19] Pickart CM, Eddins MJ. Ubiquitin: structures, functions, mechanisms. Biochim Biophys Acta 2004;1695:55–72. doi:10.1016/j.bbamcr.2004.09.019.

[20] Roos-Mattjus P, Sistonen L. The ubiquitin-proteasome pathway. Ann Med 2004;36:285–95.

[21] Komander D, Rape M. The Ubiquitin Code. Annu Rev Biochem 2012;81:203–29. doi:10.1146/annurev-biochem-060310-170328.

[22] Yau R, Rape M. The increasing complexity of the ubiquitin code. Nat Cell Biol 2016;18:579–86. doi:10.1038/ncb3358.

[23] Akutsu M, Dikic I, Bremm A. Ubiquitin chain diversity at a glance. J Cell Sci 2016;129:875–80. doi:10.1242/jcs.183954.

[24] Winter GE, Buckley DL, Paulk J, Roberts JM, Souza A, Dhe-Paganon S, et al.

Phthalimide conjugation as a strategy for in vivo target protein degradation. Science 2015;348:1376–81. doi:10.1126/science.aab1433.

[25] Fulcher LJ, Macartney T, Bozatzi P, Hornberger A, Rojas-Fernandez A, Sapkota GP. An affinity-directed protein missile system for targeted proteolysis. Open Biol 2016;6. doi:10.1098/rsob.160255.

[26] Fulcher LJ, Hutchinson LD, Macartney TJ, Turnbull C, Sapkota GP. Targeting endogenous proteins for degradation through the affinity-directed protein missile system. Open Biol 2017;7. doi:10.1098/rsob.170066.

[27] The UniProt Consortium. UniProt: a worldwide hub of protein knowledge. Nucleic Acids Res 2019;47:D506–15. doi:10.1093/nar/gky1049.

[28] Madeira F, Park YM, Lee J, Buso N, Gur T, Madhusoodanan N, et al. The EMBL-EBI search and sequence analysis tools APIs in 2019. Nucleic Acids Res 2019;47:W636–41. doi:10.1093/nar/gkz268.

[29] Waterhouse AM, Procter JB, Martin DMA, Clamp M, Barton GJ. Jalview Version 2 - a multiple sequence alignment editor and analysis workbench. Bioinformatics 2009;25:1189–91. doi:10.1093/bioinformatics/btp033.

[30] Livak KJ, Schmittgen TD. Analysis of Relative Gene Expression Data Using Real-Time Quantitative PCR and the 2−ΔΔCT Method. Methods 2001;25:402–8. doi:10.1006/meth.2001.1262.

[31] Fulcher LJ, He Z, Mei L, Macartney TJ, Wood NT, Prescott AR, et al. FAM83D directs protein kinase CK1α to the mitotic spindle for proper spindle positioning. EMBO Rep 2019:e47495. doi:10.15252/embr.201847495.

[32] Waters AM, Ozkan-Dagliyan I, Vaseva A V, Fer N, Strathern LA, Hobbs GA, et al. Evaluation of the selectivity and sensitivity of isoform- and mutation-specific RAS antibodies. Sci Signal 2017;10:eaao3332. doi:10.1126/scisignal.aao3332.

[33] Reynolds AB, Daniel J, Mccrea PD, Wheelock MJ, Wu J, Zhang Z. Identification of a New Catenin: the Tyrosine Kinase Substrate pl20cas Associates with E-Cadherin Complexes. Mol Cell Biol 1994;14:8333–42.

[34] Schatz G, Butow RA. How Are Proteins Imported into Mitochondria? Cell 1983;32:316–8.

[35] Yu F, White SB, Zhao Q, Lee FS. HIF-1alpha binding to VHL is regulated by stimulus-sensitive proline hydroxylation. Proc Natl Acad Sci U S A 2001;98:9630–5. doi:10.1073/pnas.181341498.

[36] Spencer-Smith R, Koide A, Zhou Y, Eguchi RR, Sha F, Gajwani P, et al. Inhibition of RAS function through targeting an allosteric regulatory site. Nat Chem Biol 2017;13:62–8. doi:10.1038/nchembio.2231.

[37] Morandi L, de Biase D, Visani M, Cesari V, De Maglio G, Pizzolitto S, et al. Allele Specific Locked Nucleic Acid Quantitative PCR (ASLNAqPCR): An Accurate and Cost-Effective Assay to Diagnose and Quantify KRAS and BRAF Mutation. PLoS One 2012;7:e36084. doi:10.1371/journal.pone.0036084.

[38] Tan YH, Liu Y, Eu KW, Ang PW, Li WQ, Tellez MS, et al. Detection of BRAF V600E mutation by pyrosequencing. Pathology 2008;40:295–8. doi:10.1080/00313020801911512.

[39] Cox AD, Der CJ. Ras history: The saga continues. Small GTPases 2010;1:2–27. doi:10.4161/sgtp.1.1.12178.

[40] Janes MR, Zhang J, Li L-S, Hansen R, Peters U, Guo X, et al. Targeting KRAS Mutant Cancers with a Covalent G12C-Specific Inhibitor. Cell 2018;172:578–89. doi:10.1016/j.cell.2018.01.006.

[41] Patricelli MP, Janes MR, Li L-S, Hansen R, Peters U, Kessler L V, et al. Selective Inhibition of Oncogenic KRAS Output with Small Molecules Targeting

747 the Inactive State. Cancer Discov 2016;6:316–29. doi:10.1158/2159-8290.CD-
748 15-1105.
749 [42] McCarthy MJ, Pagba C V., Prakash P, Naji AK, van der Hoeven D, Liang H, et
750 al. Discovery of High-Affinity Noncovalent Allosteric KRAS Inhibitors That
751 Disrupt Effector Binding. ACS Omega 2019;4:2921–30.
752 doi:10.1021/acsomega.8b03308.
753 [43] Kessler D, Gmachl M, Mantoulidis A, Martin LJ, Zoephel A, Mayer M, et al.
754 Drugging an undruggable pocket on KRAS. Proc Natl Acad Sci
755 2019;116:15823–9. doi:10.1073/pnas.1904529116.
756 [44] Lindsay CR, Blackhall FH. Direct Ras G12C inhibitors: crossing the rubicon. Br
757 J Cancer 2019;121:197–8. doi:10.1038/s41416-019-0499-1.
758 [45] Guillard S, Kolasinska-Zwierz P, Debreczeni J, Breed J, Zhang J, Bery N, et al.
759 Structural and functional characterization of a DARPin which inhibits Ras
760 nucleotide exchange. Nat Commun 2017;8:16111. doi:10.1038/ncomms16111.
761 [46] Spencer-Smith R, Li L, Prasad S, Koide A, Koide S, O'Bryan JP. Targeting the
762 α4-α5 interface of RAS results in multiple levels of inhibition. Small GTPases
763 2017;1248:1–10. doi:10.1080/21541248.2017.1333188.
764 [47] Koide A, Bailey CW, Huang X, Koide S. The fibronectin type III domain as a
765 scaffold for novel binding proteins. J Mol Biol 1998;284:1141–51.
766 doi:10.1006/JMBI.1998.2238.
767 [48] Khan I, Spencer-Smith R, O'Bryan JP. Targeting the α4–α5 dimerization
768 interface of K-RAS inhibits tumor formation in vivo. Oncogene 2019;38:2984–
769 93. doi:10.1038/s41388-018-0636-y.
770 [49] Tsai FD, Lopes MS, Zhou M, Court H, Ponce O, Fiordalisi JJ, et al. K-Ras4A
771 splice variant is widely expressed in cancer and uses a hybrid membrane-

772 targeting motif. Proc Natl Acad Sci 2015;112:779–84.
773 doi:10.1073/pnas.1412811112.
774 [50] Schmick M, Vartak N, Papke B, Kovacevic M, Truxius DC, Rossmannek L, et
775 al. KRas Localizes to the Plasma Membrane by Spatial Cycles of
776 Solubilization, Trapping and Vesicular Transport. Cell 2014;157:459–71.
777 doi:10.1016/j.cell.2014.02.051.
778 [51] Hu Y, Lu W, Chen G, Wang P, Chen Z, Zhou Y, et al. K-ras G12V
779 transformation leads to mitochondrial dysfunction and a metabolic switch from
780 oxidative phosphorylation to glycolysis. Cell Res 2012;22:399–412.
781 doi:10.1038/cr.2011.145.
782 [52] Goodwin JS, Drake KR, Rogers C, Wright L, Lippincott-Schwartz J, Philips
783 MR, et al. Depalmitoylated Ras traffics to and from the Golgi complex via a
784 nonvesicular pathway. J Cell Biol 2005;170:261–72.
785 doi:10.1083/jcb.200502063.
786 [53] Symonds JM, Ohm AM, Tan A-C, Reyland ME. PKCδ regulates integrin αVβ3
787 expression and transformed growth of K-ras dependent lung cancer cells.
788 Oncotarget 2016;7:17905–19. doi:10.18632/oncotarget.7560.
789 [54] Singh A, Greninger P, Rhodes D, Koopman L, Violette S, Bardeesy N, et al. A
790 Gene Expression Signature Associated with “K-Ras Addiction” Reveals
791 Regulators of EMT and Tumor Cell Survival. Cancer Cell 2009;15:489–500.
792 doi:10.1016/j.ccr.2009.03.022.
793 [55] Singh A, Sweeney MF, Yu M, Burger A, Greninger P, Benes C, et al. TAK1
794 Inhibition Promotes Apoptosis in KRAS-Dependent Colon Cancers. Cell
795 2012;148:639–50. doi:10.1016/j.cell.2011.12.033.
796

Figure Legends

Figure 1 – Generation of GFP-KRAS knockin in A549 NSCLC cells by CRISPR/Cas9.

(A) Sequence Alignment of RAS protein isoforms K-RAS4A (Uniprot-ID: P01116-1), K-RAS4B (P01116-2), H-RAS (P01112-1) and N-RAS (P01111-1). Degrees of shading according to % sequence identity between the four proteins. Asterisk denotes frequently mutated G12 position. (B) A549 WT or K-RAS$^{GFP/GFP}$ knock-in (KI; hereafter called A549^{GFPKRAS}) cell lysates were separated by SDS PAGE and the indicated antibodies were used for detection by Western blotting. Arrows indicate different RAS species (black: endogenous K-RAS; dark grey: GFP-K-RAS; light grey: H-/N-RAS). (C) Lysates were processed as in (B) and subjected to immunoprecipitation with GFP-trap beads. I = Input, Ft = Flowthrough, E = Elution. (D) Widefield immunofluorescence microscopy of untreated A549^{GFPKRAS} cells labelled with antibodies specific for GFP (all left panels, cyan) and P120 (top two middle panels, magenta) or ATPB (bottom two middle panels, magenta), and DAPI (all left and middle panels, blue). Overlay of GFP and P120/ATPB is shown on the right. Scalebar = 10μm. Two representative images for each staining are shown. All blots are representative of at least 3 independent experiments.

Figure 2 – AdPROM mediated degradation of GFP-K-RAS

(A) Schematic representation of the proteolytic AdPROM system. The high affinity

GFP-binder aGFP16 is fused to VHL, which is recruited by EloB and EloC to Cul2. aGFP16 recruits GFP-tagged K-RAS and presents it in close proximity to RBX1 in the assembled Cul2 complex. Ubiquitin (Ub) is transferred onto K-RAS, which is subsequently degraded (dashed lines and faded). (B) After treatment with retroviruses and selection, cell lysates of indicated cell lines were separated on SDS PAGE and analysed by Western blotting using the indicated antibodies. (C) Indicated cell lines were treated with 1 μM MLN4924 in 0.1% DMSO, or just DMSO at 0.1% for 24 h. Samples were further processed as in (B). (D) Indicated cell lines were analysed on a Canto flow cytometer. Shown populations were preselected for cells and single cells before defining the gate for GFP positive cells (shown). GFP-A is plotted against PE-A in all cases. Numbers indicate percentage of cells within the respective gate. (E) Histogram representation of plots in (D). KI = A549 $KRAS^{GFP/GFP}$ cells (referred to as $a549^{GFPKRAS}$ cells throughout text). Western blots are representative of at least 3 independent experiments. Flow cytometry data are representative of 2 independent experiments.

Figure 3 – Degradation of endogenous RAS using a RAS-specific monobody. (A) Cell lysates of indicated cell lines were subjected to immunoprecipitation with anti-Flag beads. Input (I), Flowthrough (Ft) and precipitates (IP) were run on SDS-PAGE and subjected to Western blotting with the respective antibodies. (B), (C) and (G) SDS-PAGE and Western blots of lysates of indicated cell lines using the indicated antibodies. Samples were treated with 1 μM MLN4924 or 0.1% DMSO for 24 h (C). (D) and (E), flow cytometric analysis of indicated cells, done as in Figure 2. KI = $A549^{GFPKRAS}$ cells. (F) Widefield immunofluorescence microscopy of indicated cell lines treated with anti-GFP antibody and DAPI for staining. Scalebar = 10 μm.

Two representative images are shown for each condition. (H) 5,000 cells from (B) and (G) were grown in triplicate in 12 well dishes. After 7 days, cells were fixed and stained with crystal violet. A representative image of the replicates is shown. (I) Staining from plates in (H) was extracted by methanol and absorbance at 570 nm was measured. Plotted 570 nm values are relative to the respective untreated sample. The number of biological replicates is indicated next to the cell line name. For statistical analysis, one-way ANOVA analysis with Dunnett's multiple comparisons test was done. Comparisons were drawn to the untreated sample. Western blots and immunofluorescence data are representative of at least 3 independent experiments. Flow cytometry data are representative of 2 independent experiments.

Figure 4 – Degradation of RAS in different cell lines and effects on proliferation

Lysates of untreated (A), or retrovirally transduced cell lines (indicated expression constructs) (B) were separated by SDS PAGE and analysed by Western blotting with the indicated antibodies. Comparison of cell lines in (A) was done only once. K-RAS mutation statuses for individual cell lines are indicated in brackets. (C) 5,000 cells from (B) were grown in triplicate in 12-well dishes. After 7 days, cells were fixed and stained with crystal violet. A representative image of the replicates is shown. (D) Staining from plates in (C) was extracted by methanol and absorbance at 570 nm was measured. Plotted 570 nm values are relative to the respective untreated sample. The number of biological replicates (applies to Western blots in (B) as well) is indicated next to the cell line. For statistical analysis one-way ANOVA analysis with Dunnett's multiple comparisons test was done. Comparisons were drawn to the untreated sample.

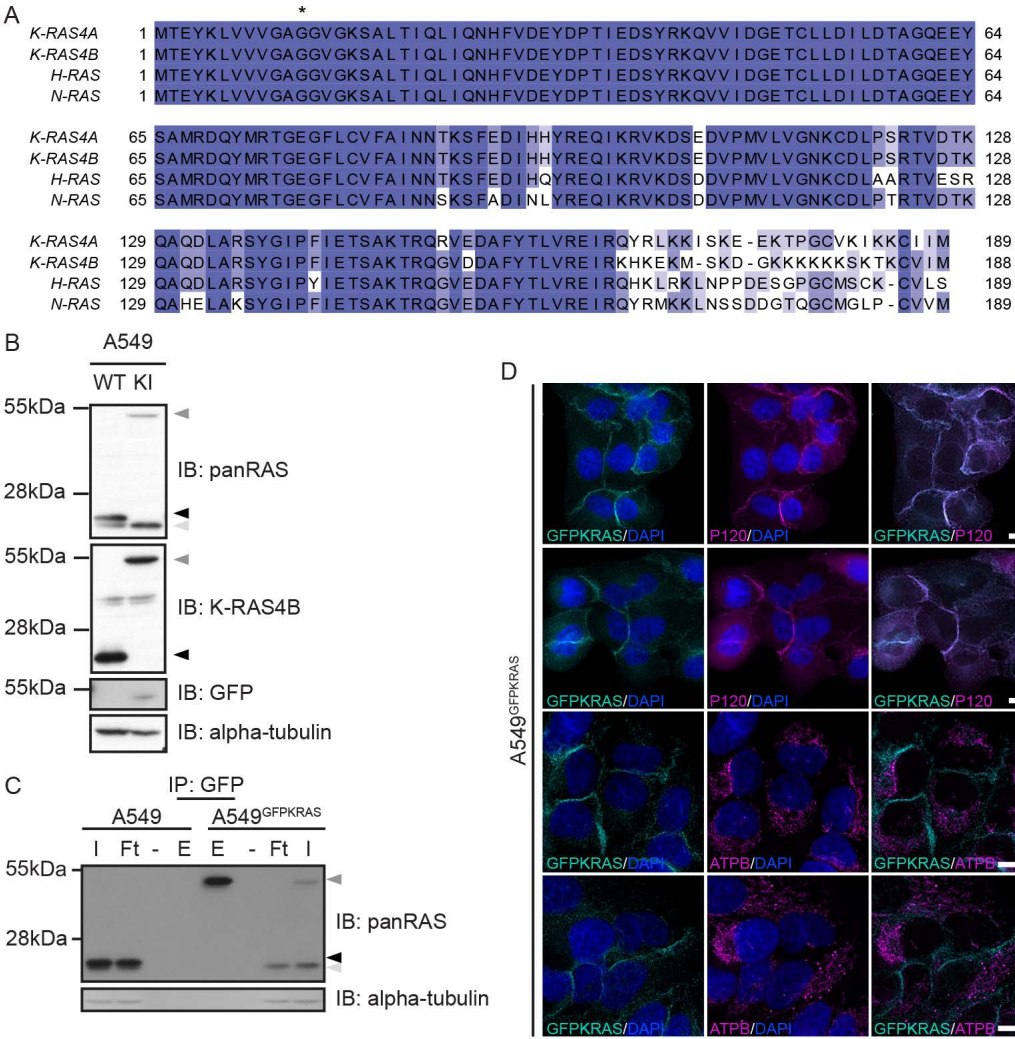

Figure 1 - Generation of GFP-KRAS knockin in A549 NSCLC cells by CRISPR/Cas9.

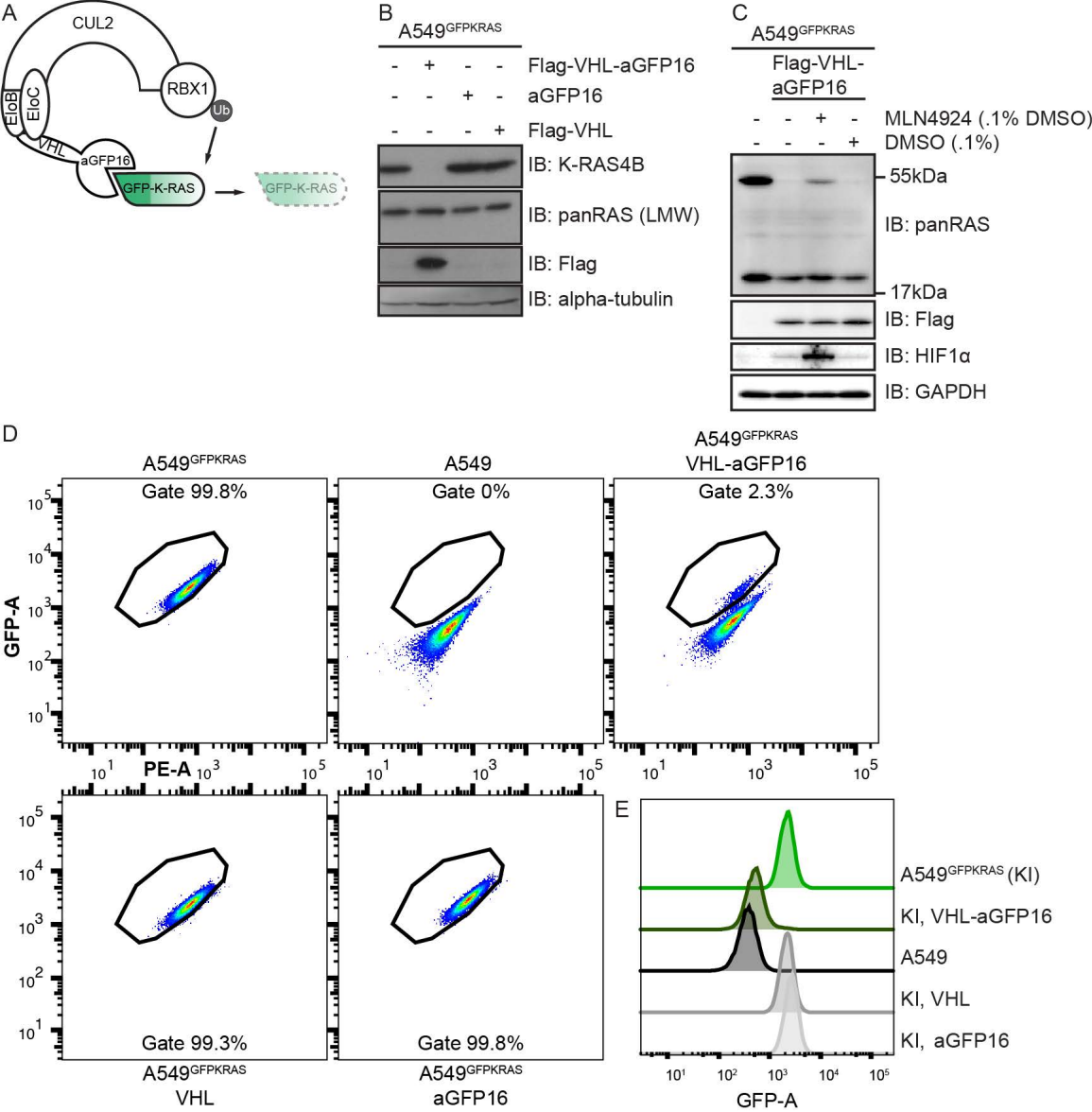

Figure 2 – AdPROM mediated degradation of GFP-K-RAS

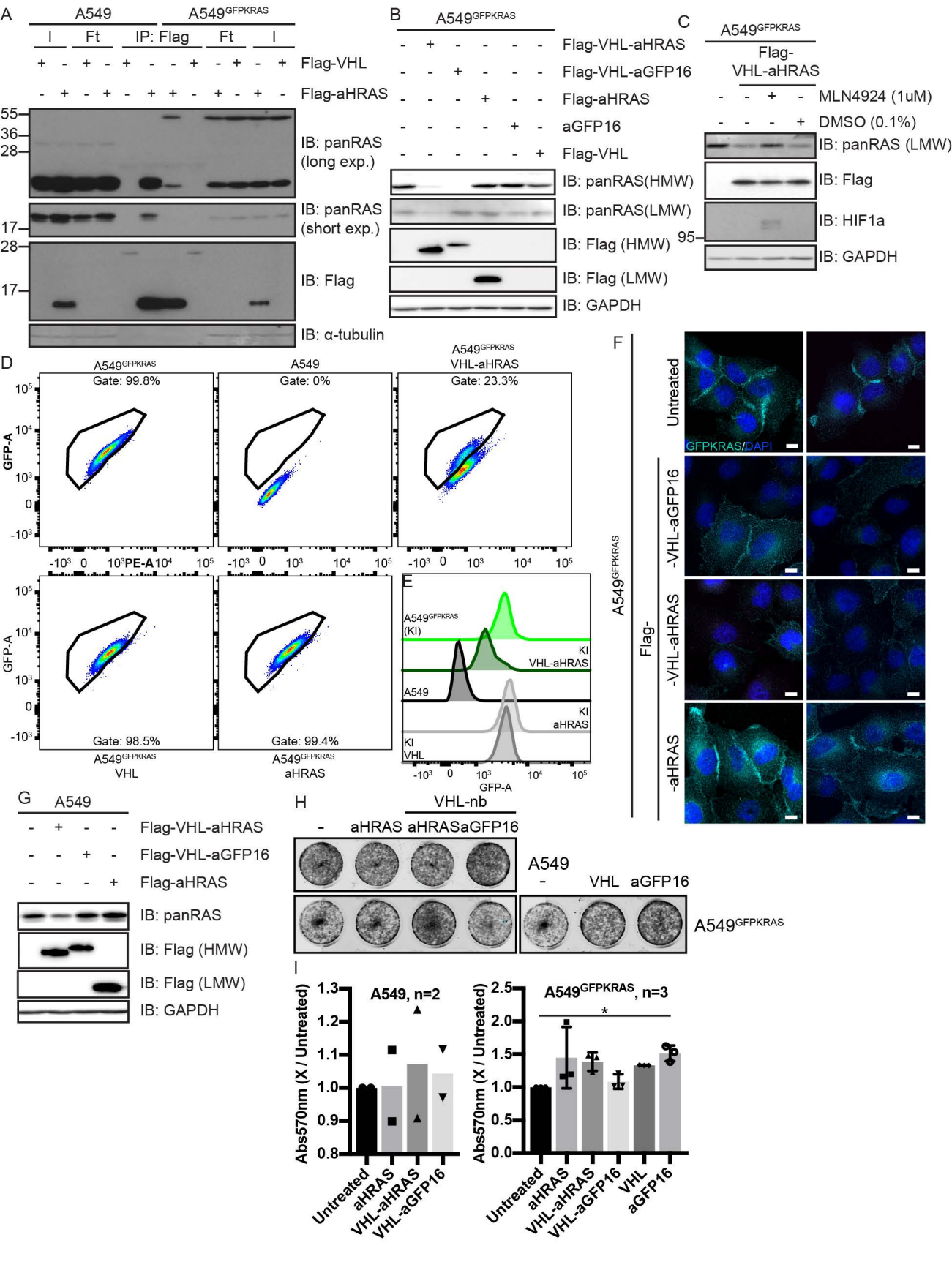

Figure 3 - Degradation of endogenous RAS using a RAS-specific monobody.

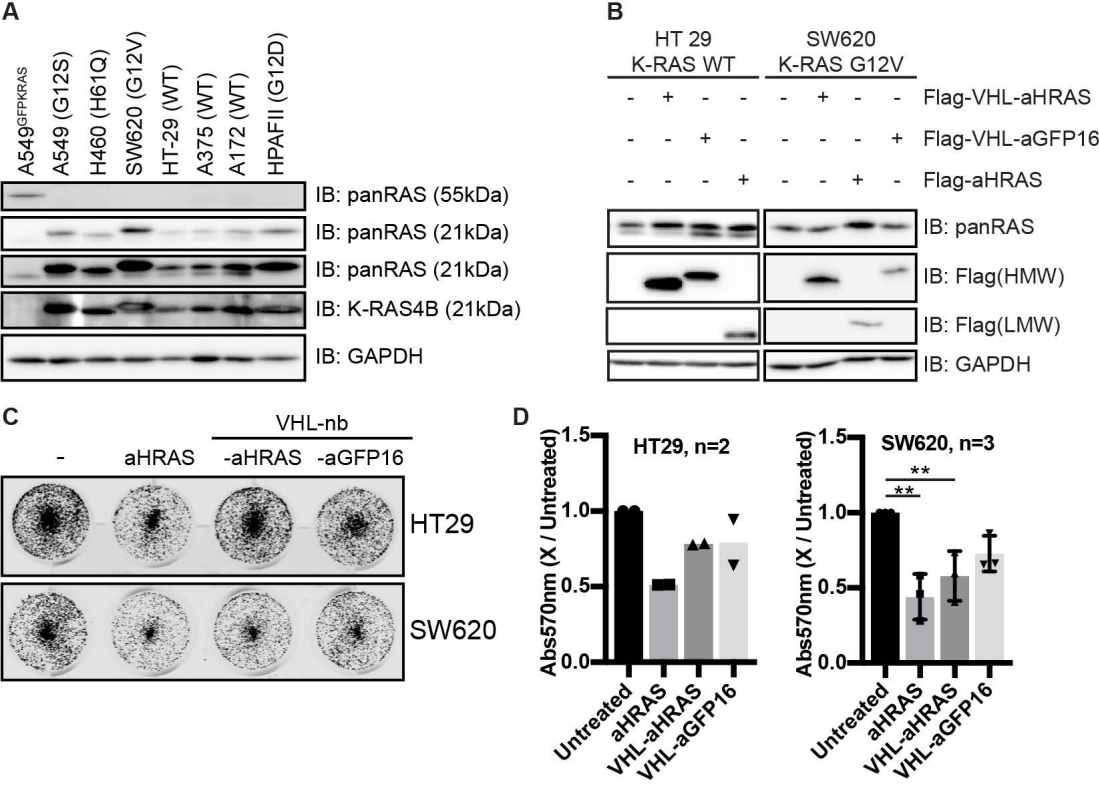

Figure 4 - Degradation of RAS in different cell lines and effects on proliferation

A

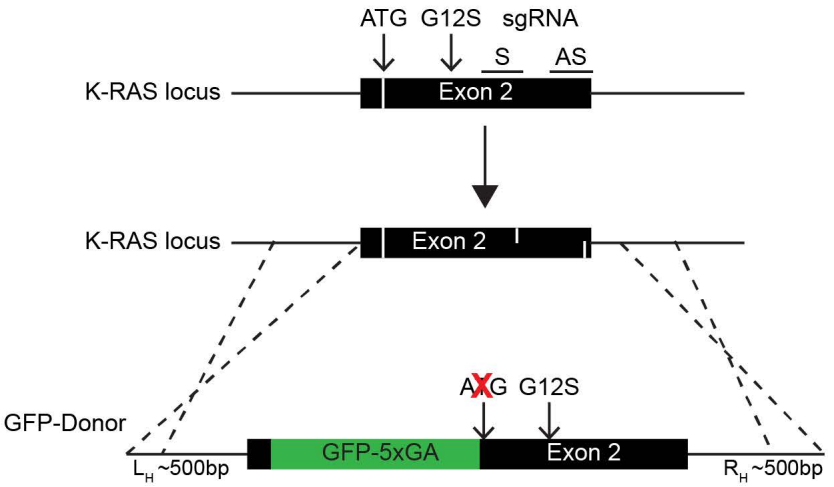

B

Codon	10	11	12	13
AA	Gly	Ala	Gly	Gly
WT	GGT	GCA	GGA	GGT
Donor	GGA	GCT	TCT	GGC
AA	Gly	Ala	Ser	Gly

C

Figure S1 - Characterization of A549^{GFPKRAS}

(A) Schematic representation of the CRISPR/Cas9 strategy used for A549 cells. Two plasmids encoding sgRNA sequences targeting the K-RAS locus on exon 2 were co-expressed with Cas9-D10A, to create two nicks in K-RAS complementary strands for a double stranded break. A donor plasmid consisting of GFP cDNA sequence without the stop codon followed by a GAGAGAGAGA linker flanked by Left and Right homology arms (L_H and R_H, respectively) was designed and co-transfected to allow homologous recombination for insertion of the GFP-5xGA tag onto the native K-RAS locus at the start codon. Consequently, the start codon of K-RAS was eliminated. (B) The indicated silent mutations on sgRNA target codons (10-13) were introduced in the donor sequence to block subsequent dsDNA breaks following integration of the donor on K-RAS locus. (C) A screenshot of DNA sequence analysis from Benchling of the resulting GFP-positive clone. Top: 14 DNA sequence files were aligned against the predicted WT RAS gene locus sequence with the GFP-fusion (indicated in light green) and the 5xGA linker. The box indicates area of the image that is magnified below. The magnified area shows DNA sequence alignment of the A549^{GFPKRAS} cell line at the site of the G12S mutation, which also shows silent mutations. The Ab1 files containing the DNA sequence chromatograms are deposited online.

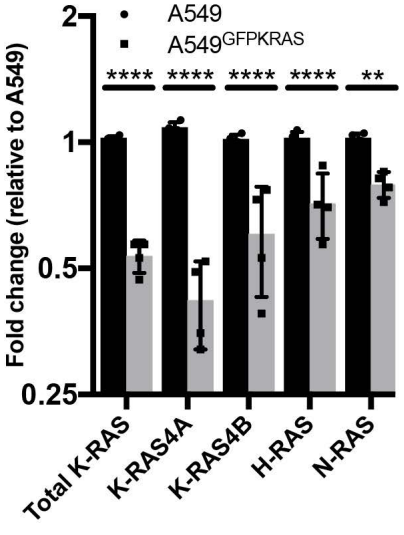

Figure S2 - Analysis of RAS transcript levels in A549 WT and A549^{GFPKRAS}

mRNA was extracted from indicated cell lines and cDNA was synthesised. Fold changes in RAS expression were calculated after qRT-PCR with specific primers between A549^{GFPKRAS} (grey bars) and A549 WT (black bars). Error bars are shown for n=4. Statistical significance was calculated with a 2-way ANOVA, Sidak's multiple comparison test.

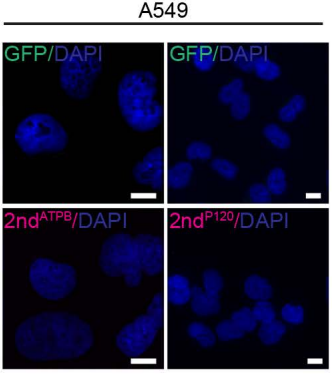

Figure S3 - Negative controls for Figure 1D
Experimental procedure is described in Figure 1D. An additional slide of A549 WT cells (GFP negative) was treated with the secondary antibody used for ATPB or P120. Exposure times are set to be the same as for the positive sample slides in Figure 1D. Scalebar = 10μm

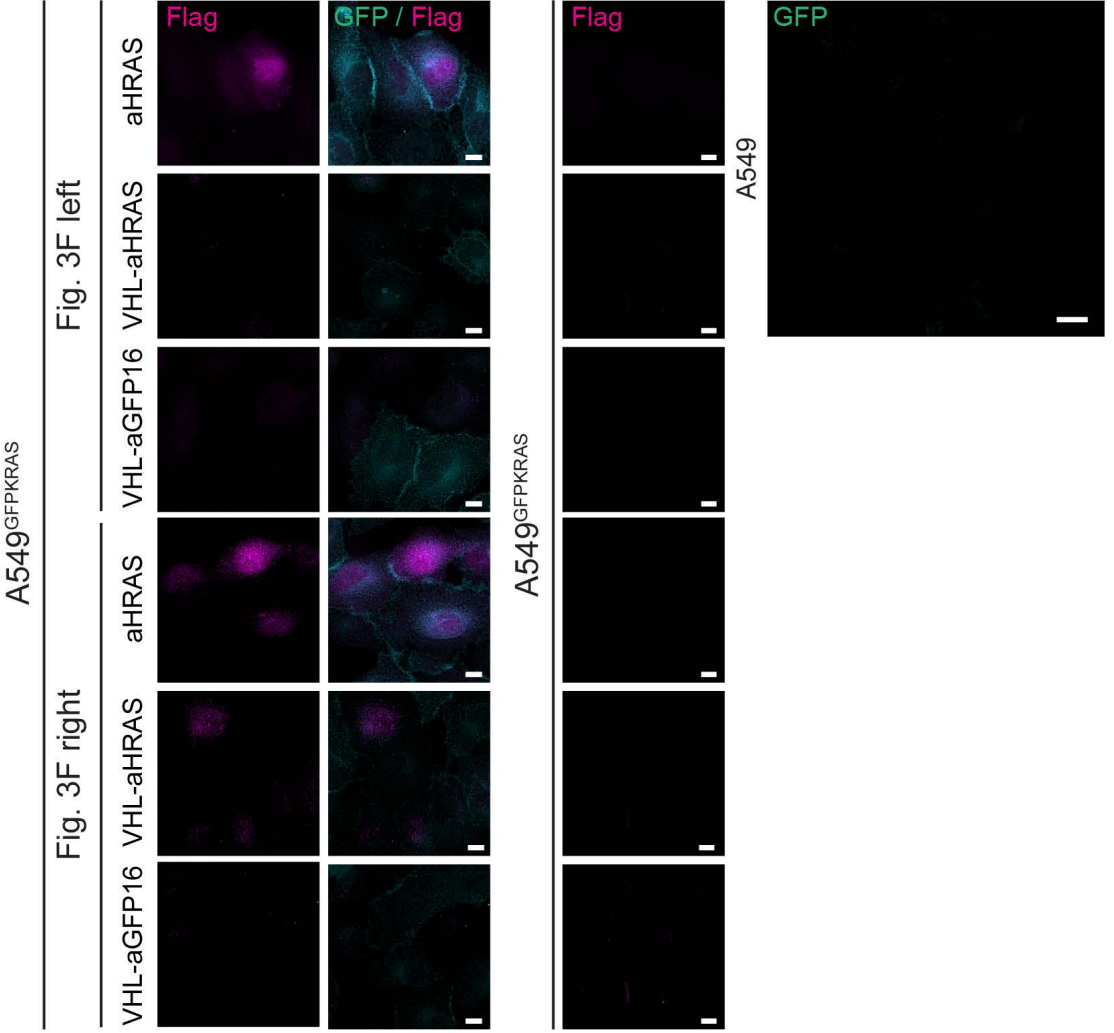

Figure S4 - FLAG signal and controls for Figure 3F.

Slides of Fig. 3F (A549^{GFPKRAS} with or without indicated transductions) were additionally stained with anti-FLAG antibody and secondary stain for detection in the 594 channel (Flag) (2 leftmost columns). The top 4 rows represent the left column of Fig. 3F, the bottom 4 rows the right column of Fig. 3F. Appropriate negative control (A549^{GFPKRAS} cells without a FLAG construct) were stained with the same antibody combination and exposure time (Column 3). Brightness and contrast for individual positive stains were background adjusted for these samples (note that the same negative sample is used for more than one picture). Additionally A549 WT cells were stained with the GFP antibody to act as negative control for GFP signal in main Figure 3F (panel on the right). Scalebar = 10µm.